Chapter 5: Observations: Oceanic Climate Change and Sea Level

Coordinating Lead Authors: Nathaniel Bindoff, Jürgen Willebrand

Lead Authors: Vincenzo Artale, Anny Cazenave, Jonathan Gregory, Sergey Gulev, Kimio Hanawa, Corinne Le Quéré, Sydney Levitus, Yukihiro Nojiri, C. Shum, Lynne Talley, Alakkat Unnikrishnan

Contributing Authors: J. Antonov, N. Bates, T.Boyer, D. Chambers, B.Chao, J. Church, S. Emerson, R. Feely, H. Garcia, M. González-Dávila, N. Gruber, S. Josey, T. Joyce, K. Kim, B. King, A. Körtzinger, K. Lambeck, K. Laval, N. Lefevre, E.Leuliette, R. Marsh, C. Mauritzen, M. McPhaden, C. Millot, C. Milly, R. Molinari, S. Nerem, T. Ono, M. Pahlow, T. Peng, A. Proshutinsky, D. Quadfasel, B. Qiu, S. Rahmstorf, S. Rintoul, M. Rixen, P. Rizzoli, C. Sabine, F. Schott, Y. Song, D. Stammer, T. Suga, C. Sweeney, M. Tamisiea, M. Tsimplis, R. Wanninkhof, J. Willis, P. Woodworth, I. Yashayaev, I. Yasuda

Review Editors: Laurent Labeyrie, David Wratt

Date of Draft: 6 March 2006

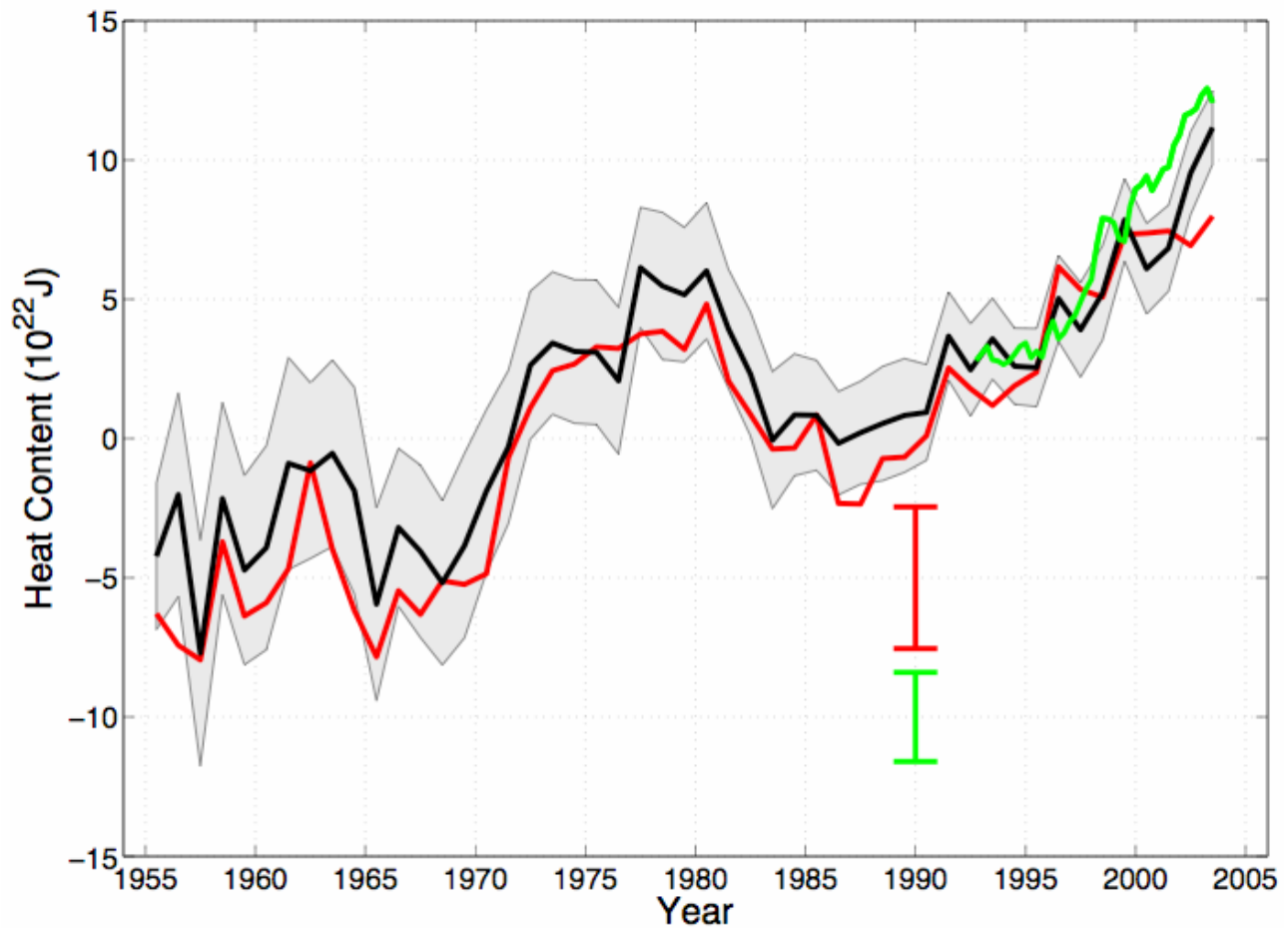**Notes:** TSU compiled version

1 **Figures**
2

3
4
5 **Figure 5.2.1.** Time series of yearly ocean heat content (10^{22} J) for the 0–700 m layer. The black curve is
6 based on Levitus et al. (2005a), with the shading representing the level of approximately 95% statistical
7 accuracy. The red and green curves are based on the analyses by Ishii et al. (2006) and Willis et al. (2004),
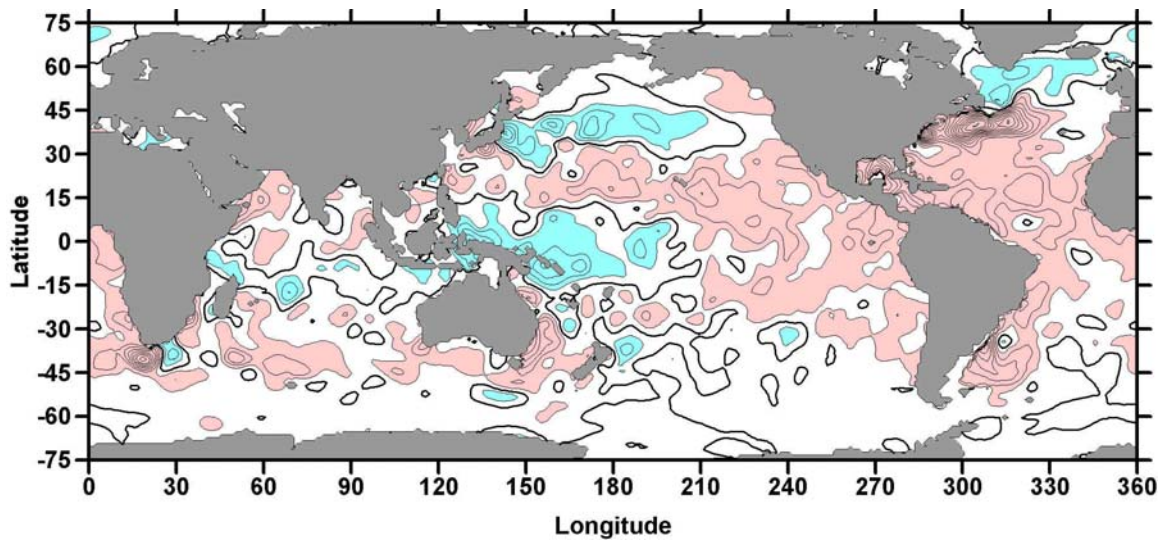8 with error bars denoting 95% confidence interval.
9

1
2

3
4
5 **Figure 5.2.2.** Linear trend (1955–2003) of ocean heat content for the 0–700 m layer from Levitus et al.
6 (2005a). Contour interval is 1×10^{17} J/year. The linear trend is computed at each grid point using a least
7 squares fit to the time series at each gridpoint. Red shading indicates values equal or greater than $1 \times$
8 10^{17} J/year and blue shading indicates values equal or less than -1×10^{17} J/year.
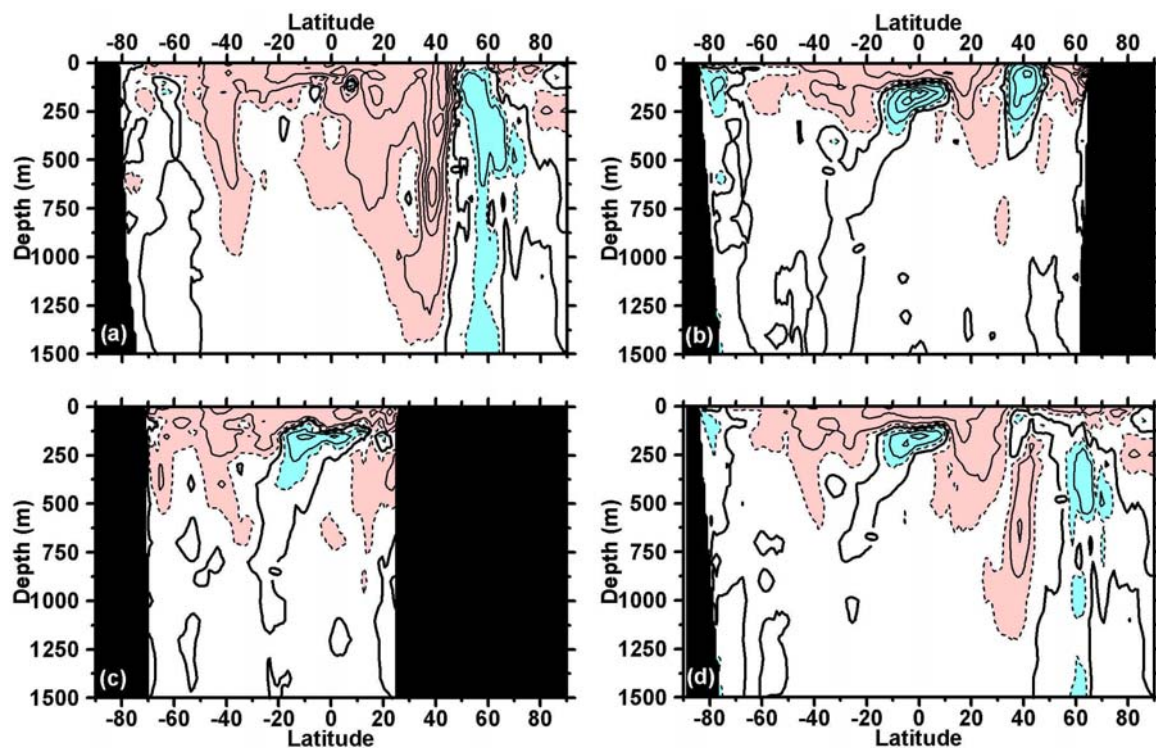9

1
2

3
4
5
6 **Figure 5.2.3.** Linear trend (1955–2003) of zonally averaged temperature for: a) Atlantic Ocean, b) Pacific
7 Ocean, c) Indian Ocean, d) World Ocean. Contour interval is 0.05°C/decade. Dark, solid line is the zero
8 contour. Red shading indicates values equal or greater than 0.025°C/decade and blue shading indicates
9 values equal or less than –0.025°C/decade. From Levitus et al. (2005a).
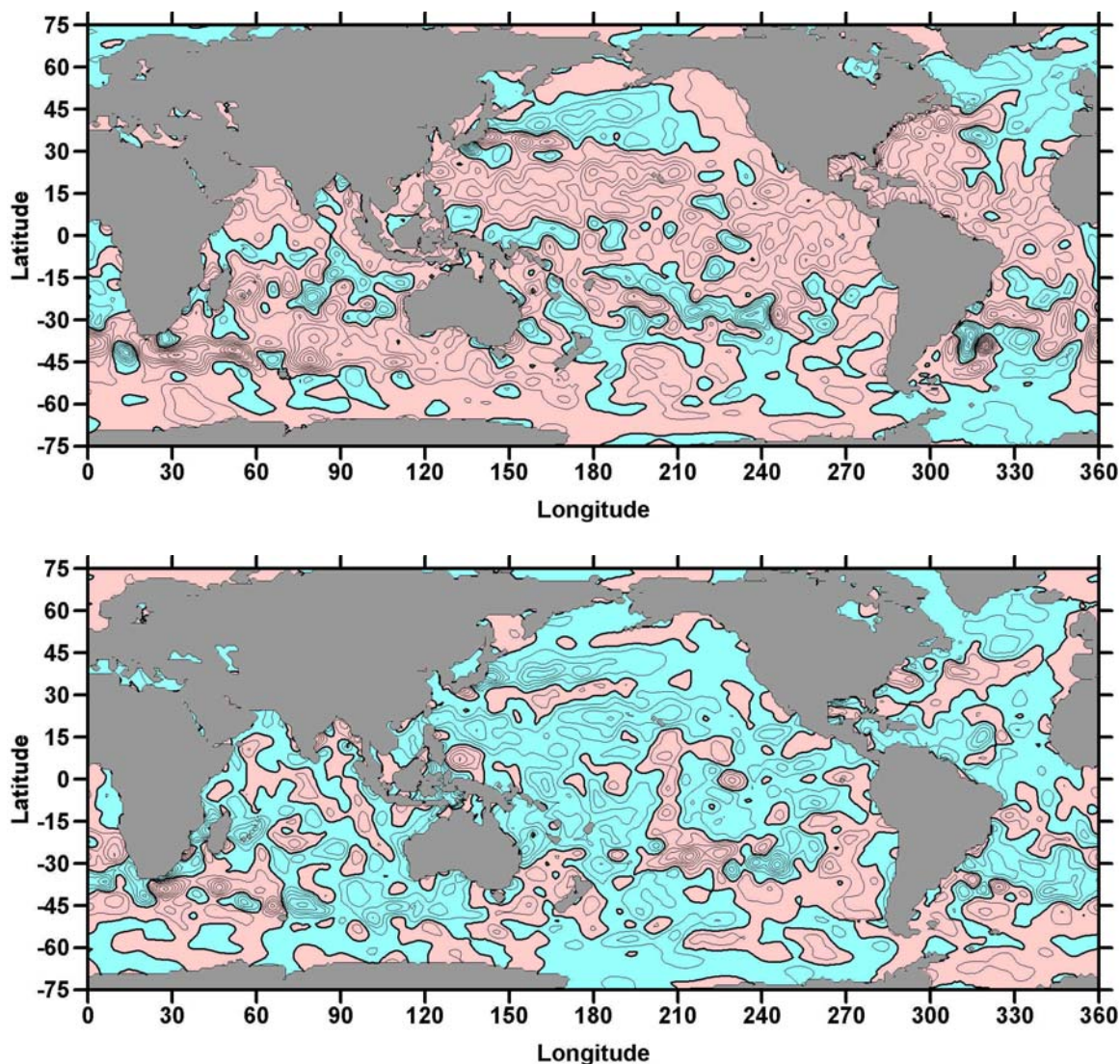10

1
2

3
4

5
6

Figure 5.2.4. Difference of ocean heat content in the 0–700 m layer over two five-year periods: (a) [(1977–1981) minus (1965–1969)] (upper panel), and (b) [(1986–1990) minus (1977–1981)] (lower panel). Contour interval is 1×10^{17} J/year. Light red shading indicates positive values and light blue indicates negative values. From Levitus et al. (2005a).

11

1
2

Energy Content Change 1961-2003 and 1993-2003 (10^{22} J)
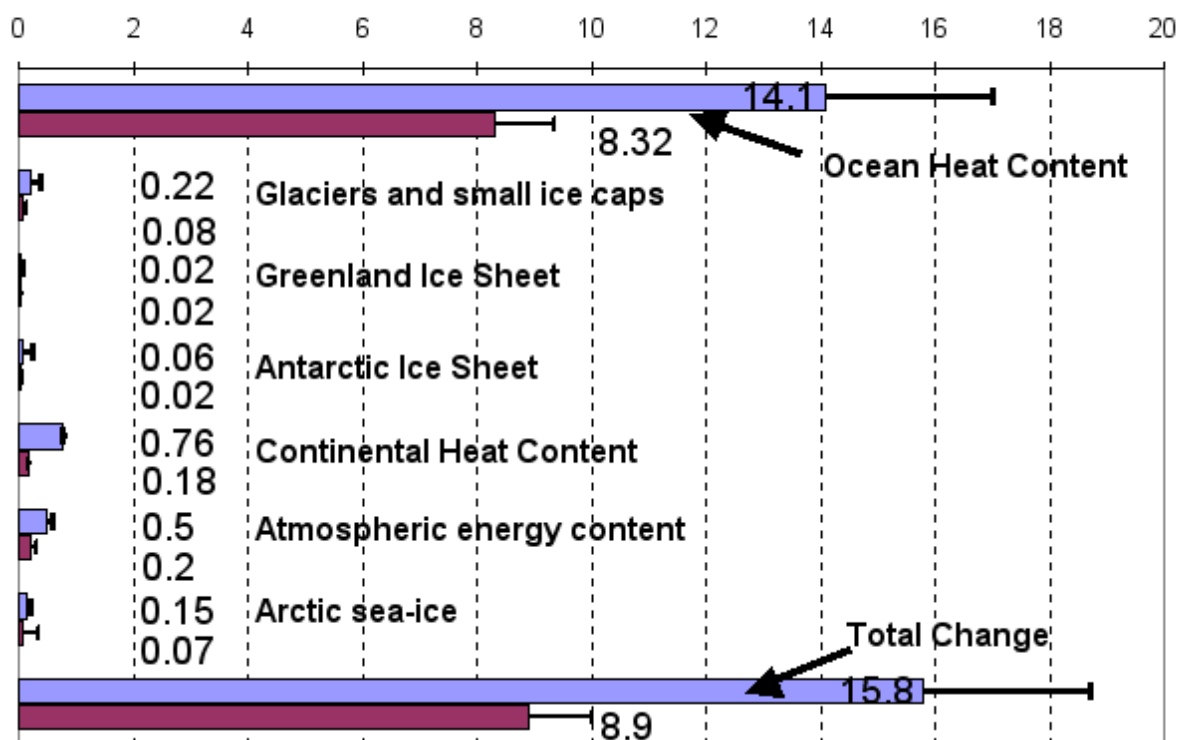

3
4
5
6   **Figure 5.2.5.** Energy content changes from differing components of the Earth Systems for two periods
7   (1961–2003) and (1993–2003). Blue bars are for1961–2003, burgundy 1993–2003. Ocean heat content
8   change from Levitus et al. (2005c), glaciers and small ice caps and Greenland and Antarctic ice sheets from
9   Chapter 4, continental heat content (Beltrami et al., 2002), atmospheric heat content (e.g., Trenberth and
10 Stepaniak, 2001) and Arctic sea-ice release (Hilmer and Lemke, 2000). Positive energy content change
11 means an increase in stored energy (or heat for oceans). All error estimates are 95% confidence intervals.
12 Note, no estimate of confidence is available for the continental heat gain. Some of the results have been
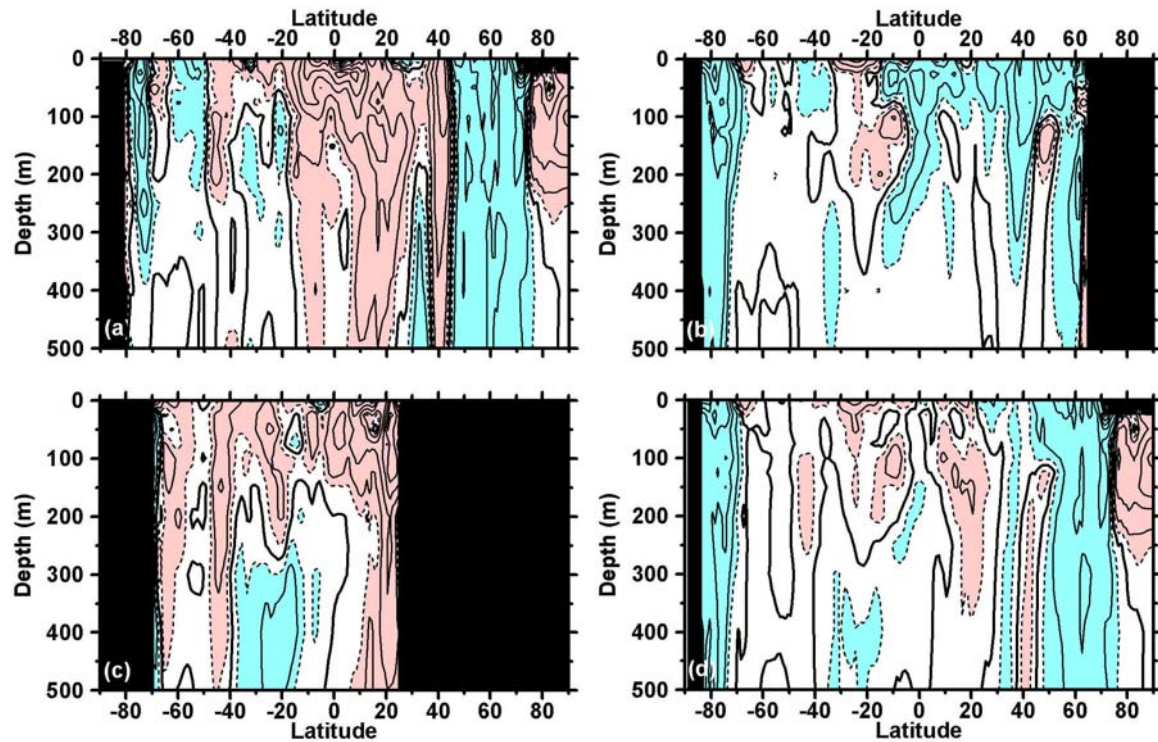13 scaled from published results for the two respective periods.
14

1
2

3
4
5 **Figure 5.2.6.** Linear trend (1955–1998) of zonally averaged salinity for: a) Atlantic Ocean, b) Pacific Ocean,
6 c) Indian Ocean, d) World Ocean. Contour interval is 0.01/decade and dashed contours are ±0.005/decade.
7 Dark, solid line is the zero contour. Red shading indicates values equal or greater than 0.005/decade and blue
8 shading indicates values equal or less than –0.005/decade. From Boyer et al. (2005).
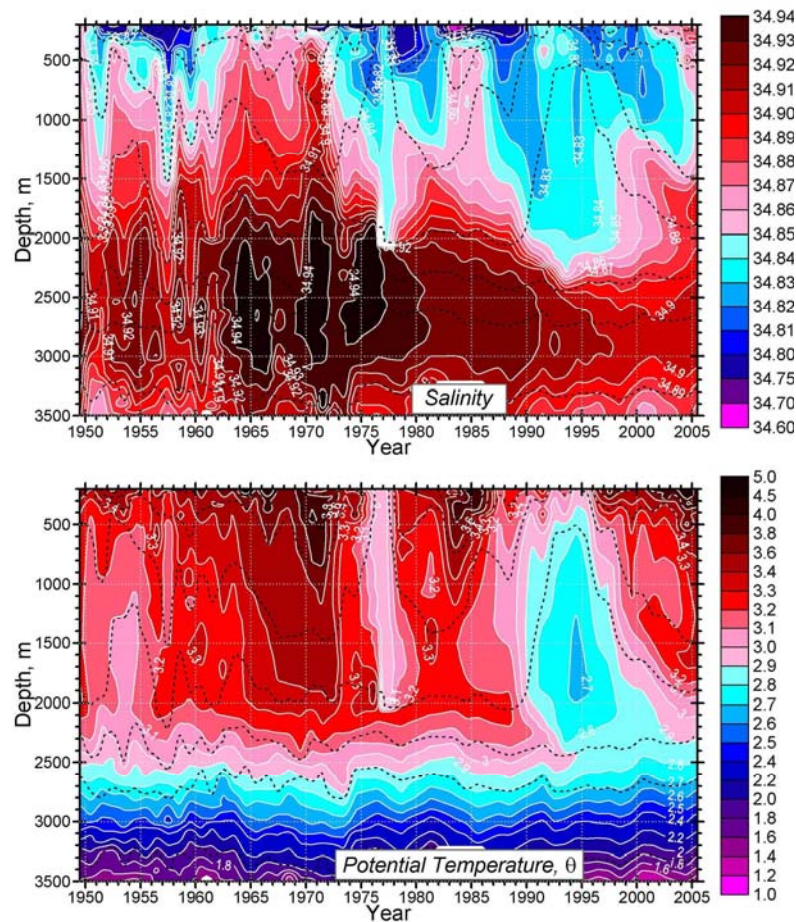9

1
2

3

Figure 5.3.1. The longest available time series of salinity (upper panel) and temperature (lower panel) in the
central Labrador Sea from 1949 to 2005 (updated from Yashayaev et al., 2003). This 56 year time series is
unique and shows that the Labrador sea was getting saltier prior to 1965 and been steadily freshening ever
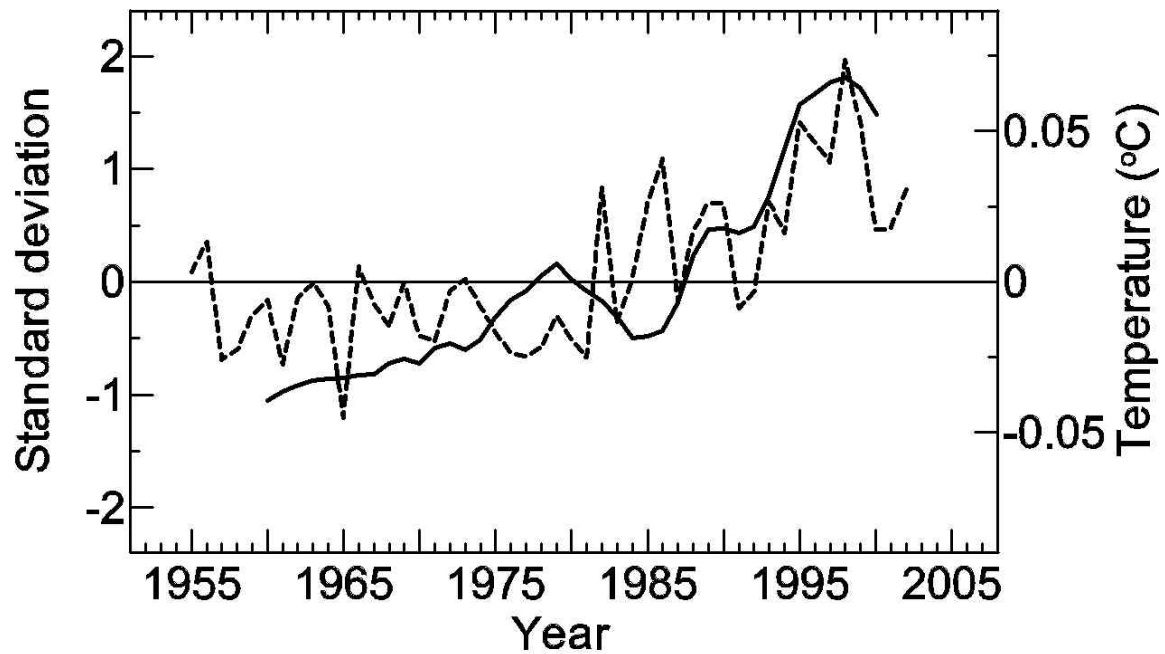since.

8

1
2

3
4
5 **Figure 5.3.2.** Time series of the Western Mediterranean Deep Water temperature (°C) (3-year running
6 window, 600 m-bottom, solid line) from Rixen et al. (2005) and annual values (dashed line) of the
7 normalized Atlantic Water Core temperature (AWCT) anomalies (average of 10 subdomains of the Arctic
8 ocean. AWCT is defined as a maximum in the vertical distribution of temperature, the depth of AWCT
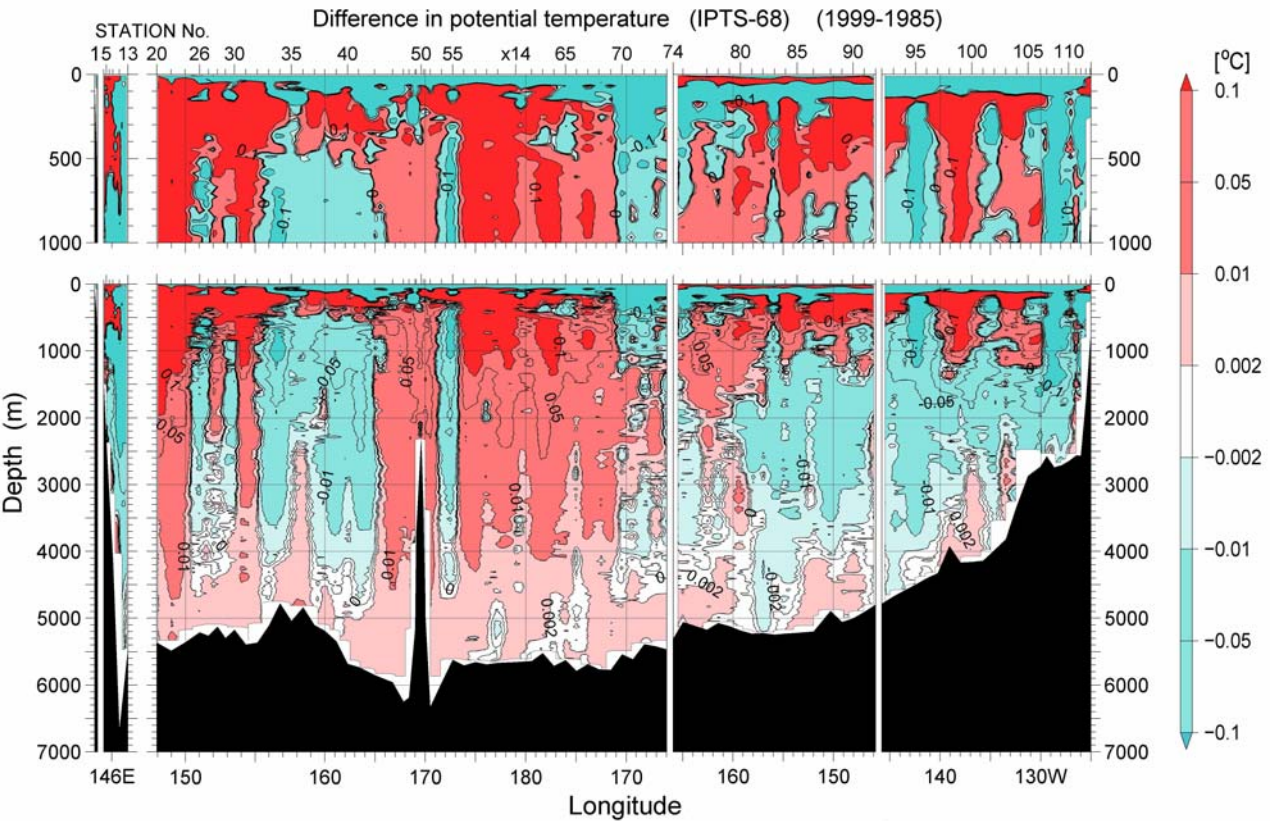9 varies from ~100 m to ~500 m) from Polyakov et al. (2004).
10

1
2

3
4 **Figure 5.3.3.** Changes in temperature below 4000 metres between 1985 and 1999 along a hydrographic
5 section across the North Pacific Ocean at a latitude of 24°N. The measurement accuracy is ~0.001°C
6 (Fukasawa et al., 2004).
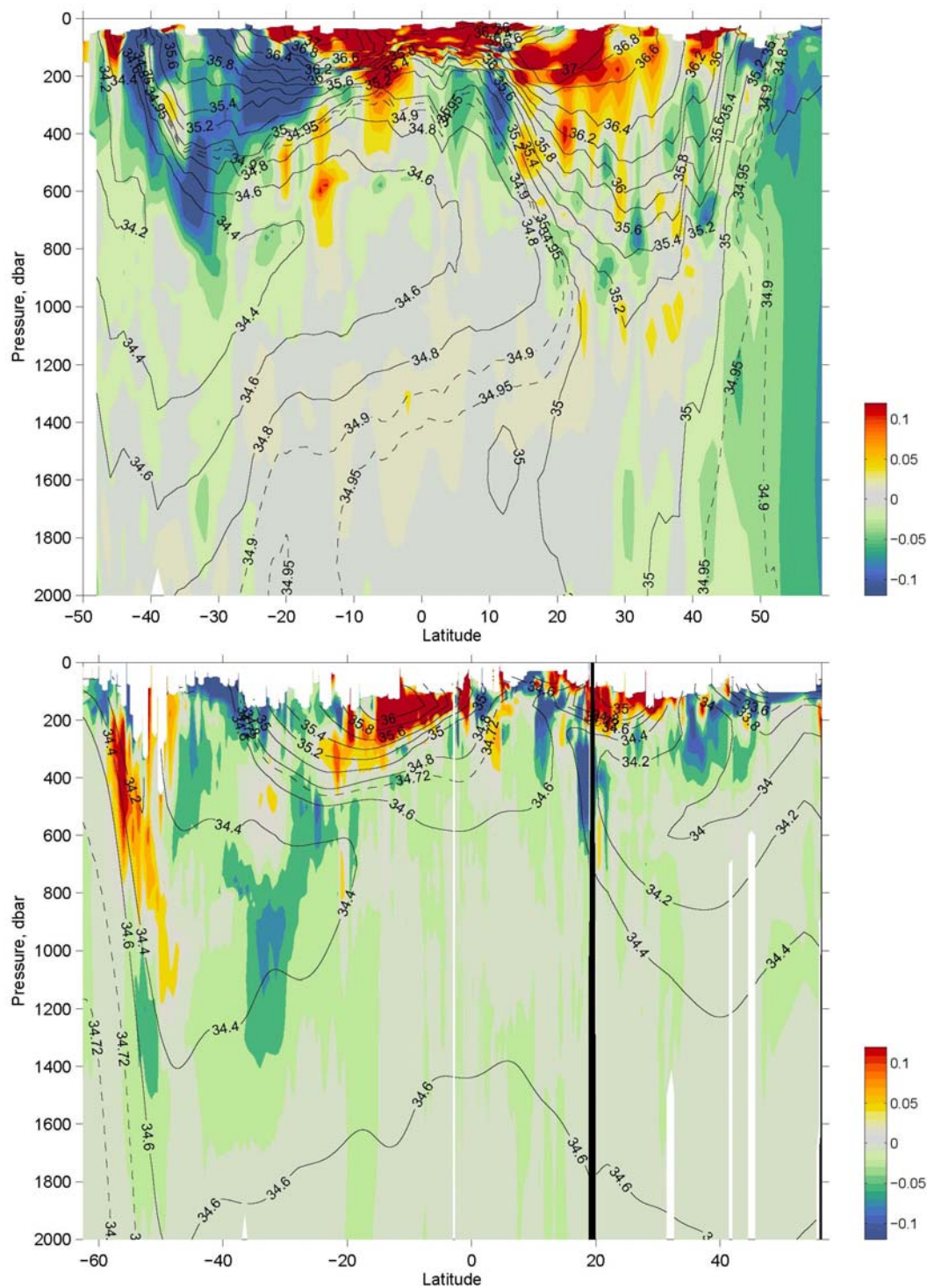
1
2

3

4
5
6 **Figure 5.3.4.** Meridional sections of differences in salinity spanning almost all of the a) Atlantic Ocean for
7 period 1985–1999 minus 1955–1969 (upper panel) and b) Pacific Ocean for WOCE 150°W Section and
8 historical data from the 1960 to 1980's (lower panel). Contours on these figures are the mean salinity fields
9 along each section and show the key features. The salinity differences are difference along isopycnals that
10 have been mapped to pressure surfaces. The Atlantic Section is along the western side of the Atlantic Ocean
11 and the Pacific section is along 150°W. The two figures are redrafted from Curry et al. (2003) and Wong et
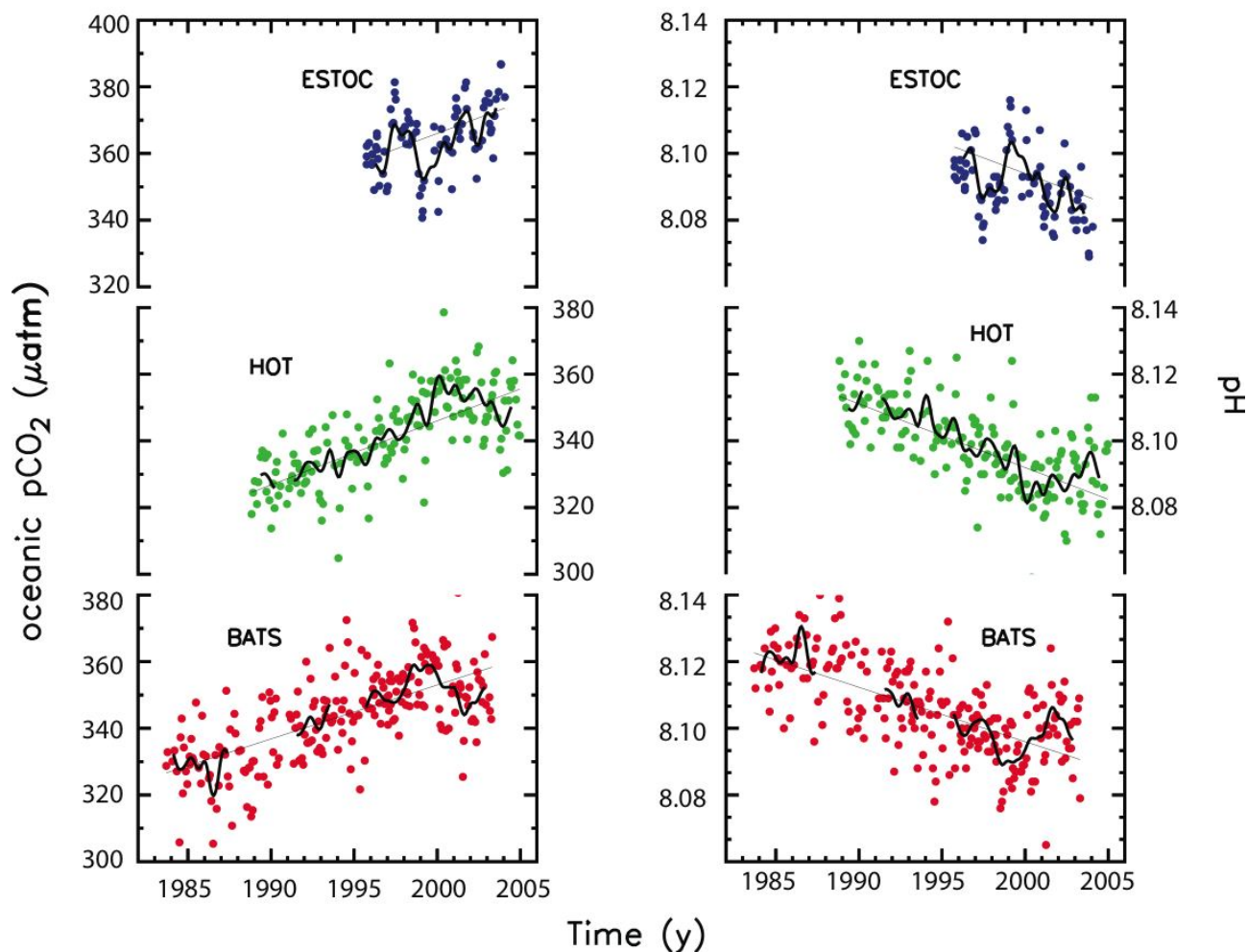12 al. (2001).

1
2

3
4
5 **Figure 5.4.1.** Changes in surface oceanic pCO_2 (left; in μatm) and pH (right) from the time-series stations at
6 ESTOC (29°N, 15°W; (Gonzalez-Dávila et al., 2003)), HOT (23°N, 158°W; (Dore et al., 2003)) and
7 BATS/Station S (31/32°N, 64°W; (Bates et al., 2002; Gruber et al., 2002)). pCO_2 and pH are directly
8 measured at ESTOC and calculated from Dissolved Inorganic Carbon and alkalinity at HOT and BATS. The
9 mean seasonal cycle was removed from all data. The thick black line filters variability less than 5 years. The
10 thin black line is a linear fit to the data, and give an increase in pCO_2 of 1.9, 1.9, and 1.6 μatm/yr and a
11 decrease in pH of 0.0018, 0.0019, and 0.0016 for ESTOC, HOT, and BATS respectively.
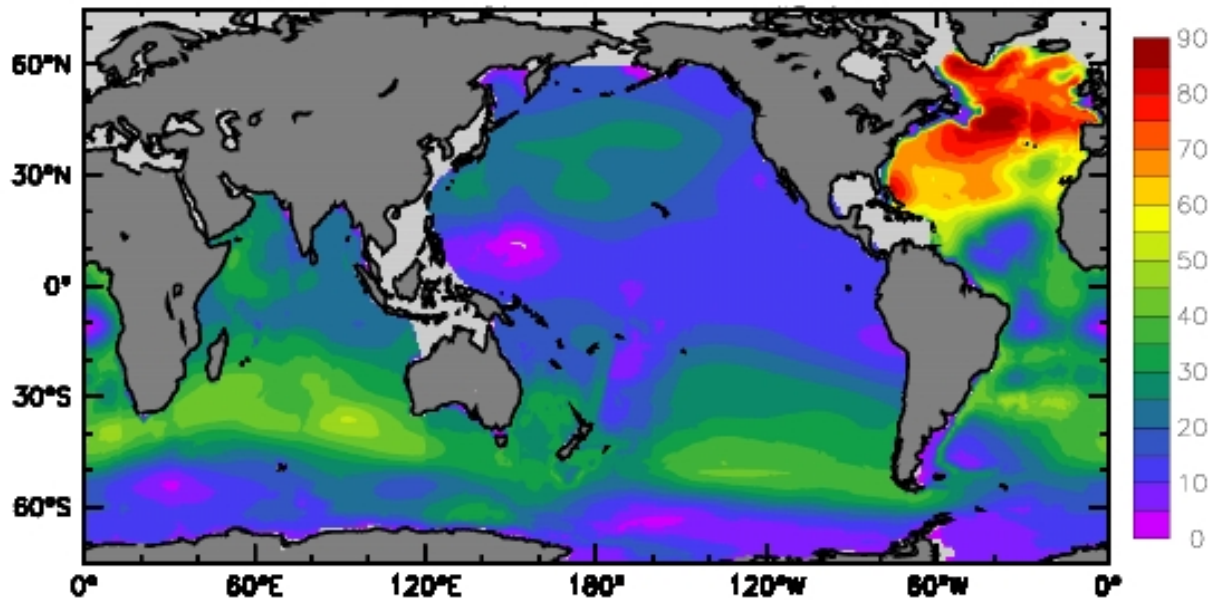12

1
2

3
4
Figure 5.4.2. Inventory of anthropogenic carbon (mol/m^2) for year 1994 from (Sabine et al., 2004).
Anthropogenic carbon is estimated indirectly by correcting the measured Dissolved Inorganic Carbon (DIC)
for the contributions of organic matter decomposition and dissolution of carbonate minerals, and taking into
account the DIC concentration the water had in the pre-industrial ocean when it was last in contact with the
atmosphere. The global inventory of anthropogenic carbon taken up by the ocean is estimated to be 118 ± 19
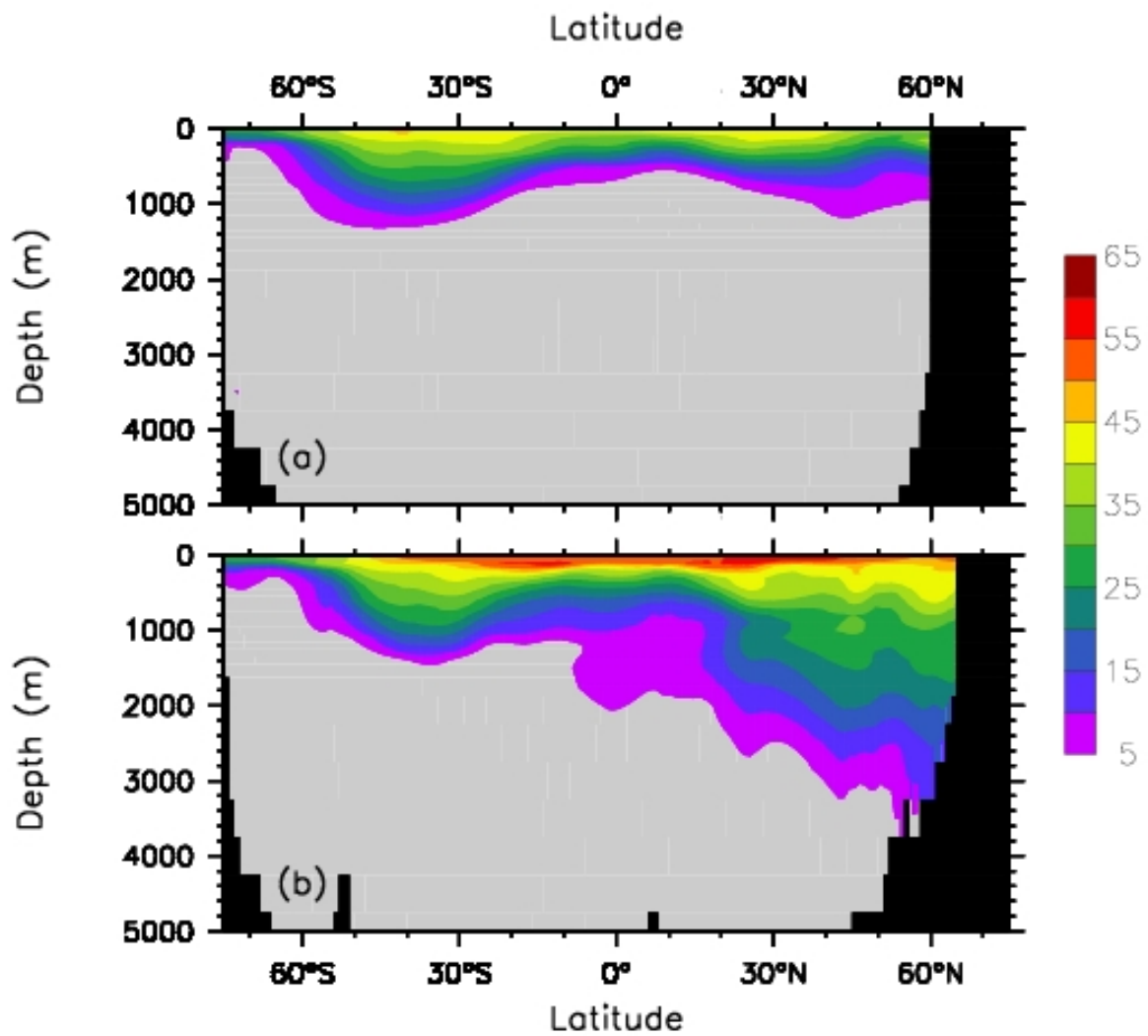GtC between 1750 and 1994.

11

1
2

3
4
5   **Figure 5.4.3.** Mean concentration of anthropogenic carbon in 1994 in μmol/kg from (Sabine et al., 2004)
6   averaged over the Pacific and Indian Oceans (top) and the Atlantic Ocean (bottom). The calculation of
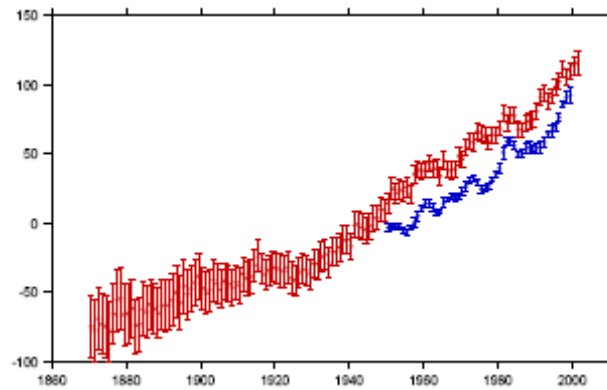7   anthropogenic carbon is described in Figure 5.4.2 and in the text.
8

1
2

3
4
5 **Figure 5.5.1.** Annual averages of the global mean sea level based on the reconstructed sea level fields since
6 1870 (red curve, updated from Church and White, 2006) and on tide gauges measurements since 1950 (blue
7 curve, from Holgate and Woodworth, 2004). Units are in mm. The blue curve has been shifted by 20 mm for
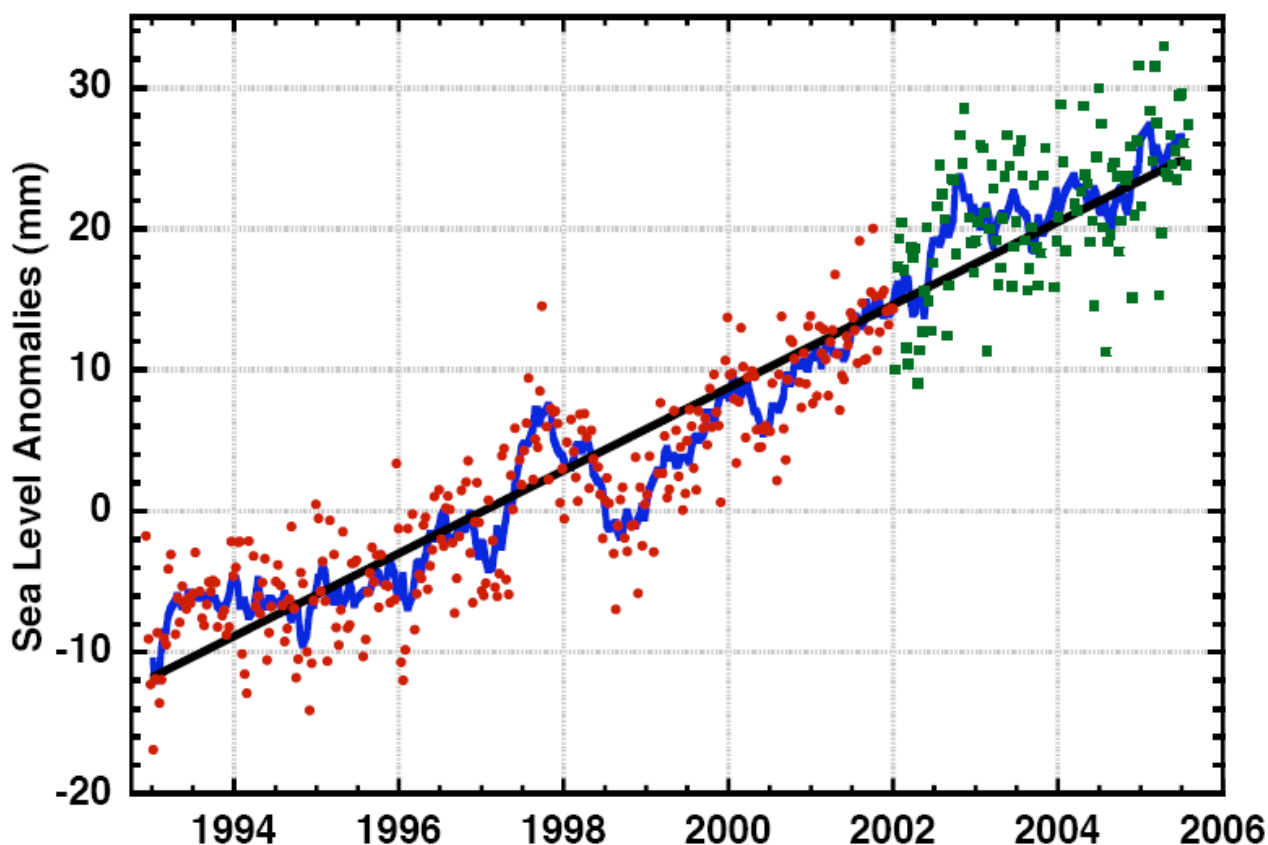8 clarity.
9

1
2

3
4
5 **Figure 5.5.2.** Variations in global mean sea level computed from satellite altimetry from January 1993 to
6 October 2005, averaged over 65°S-65°N. Dots are 10-day estimates (from Topex/Poseidon satellite in red
7 and Jason in green). The blue solid curve corresponds to 60-day smoothing and the straight line is the best
8 fitting linear trend (of 2.9 ± 0.4 mm/yr and 3.2 ± 0.4 mm/yr without and with the GIA correction). Updated
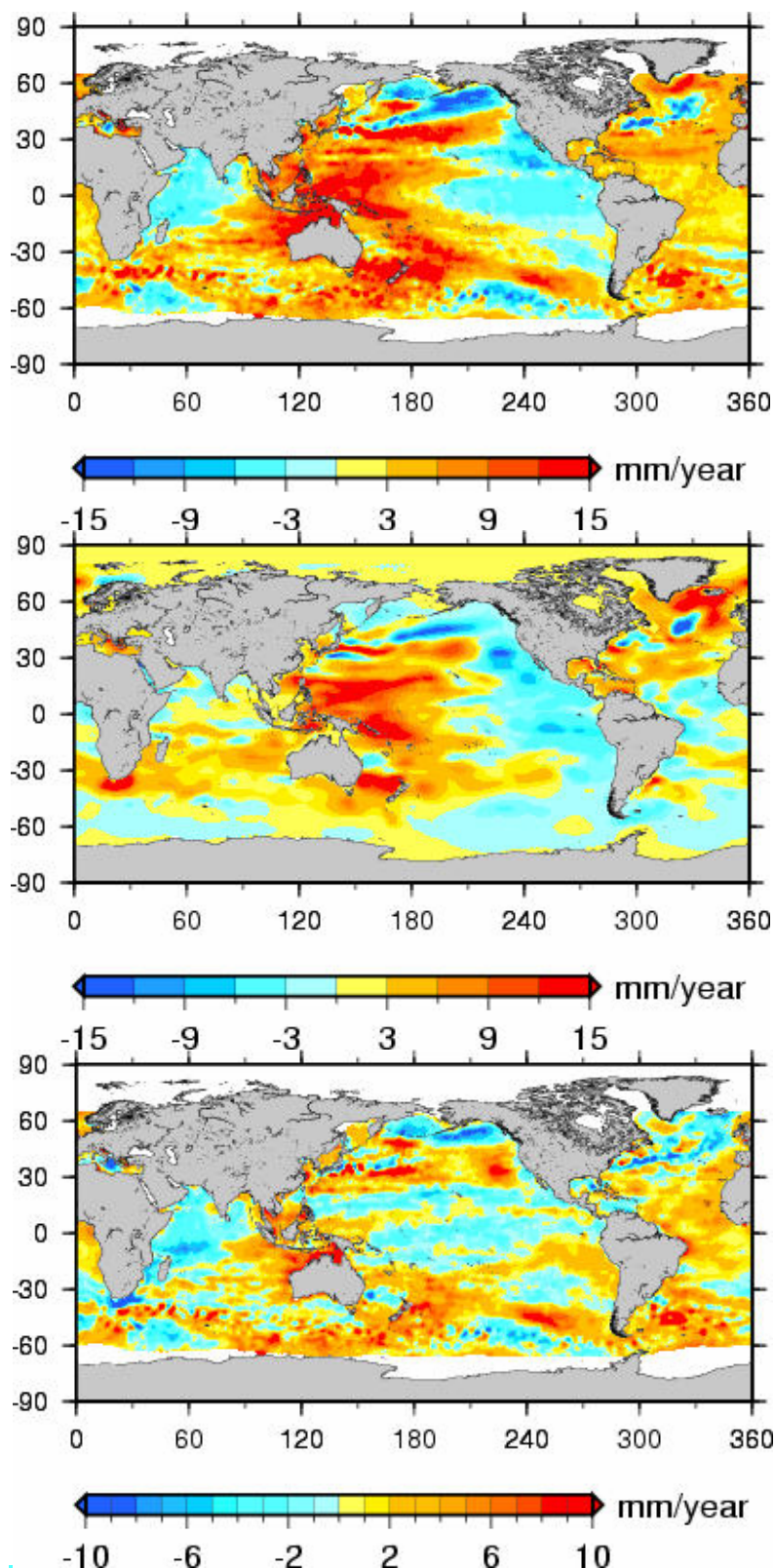9 from Cazenave and Nerem (2004) and Leuliette et al. (2004).
10

1
2

3

4

5
6
7 **Figure 5.5.3.** (a) Geographic distribution of linear trends in mean sea level for 1993–2003 based on
8 Topex/Poseidon satellite altimetry (updated from Cazenave and Nerem, 2004). Units are in mm/yr. (b)
9 Geographic distribution of linear trends in thermal expansion for 1993–2003 (based on temperature data
10 from Ishii et al., 2005, down to 700 m). Units are in mm/yr. (c) Geographic distribution of residual linear
11 trends (observed sea level trends minus thermal expansion trends) for 1993–2003. Units are in mm/yr.
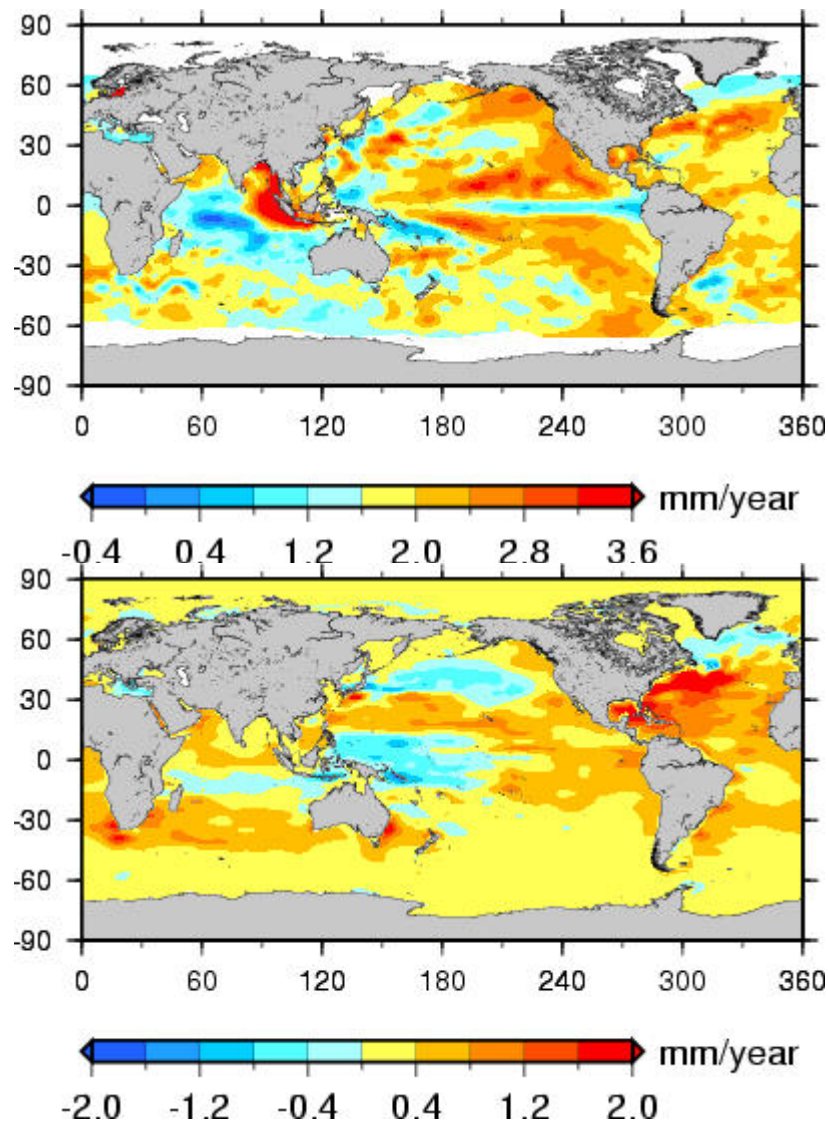12

1
2

3

4
5
6 **Figure 5.5.4.** (a) Upper figure: Geographic distribution of linear trends in mean sea level for 1955–2003
7 based on the past sea level recontruction with tide gauges and altimetry data (updated from Church et al.,
8 2004). Units are in mm/yr. (b) Lower figure: Geographic distribution of linear trends in thermal expansion
9 for 1955–2003 (based on temperature data from Ishii et al., 2005, down to 700 m). Units are in mm/yr.
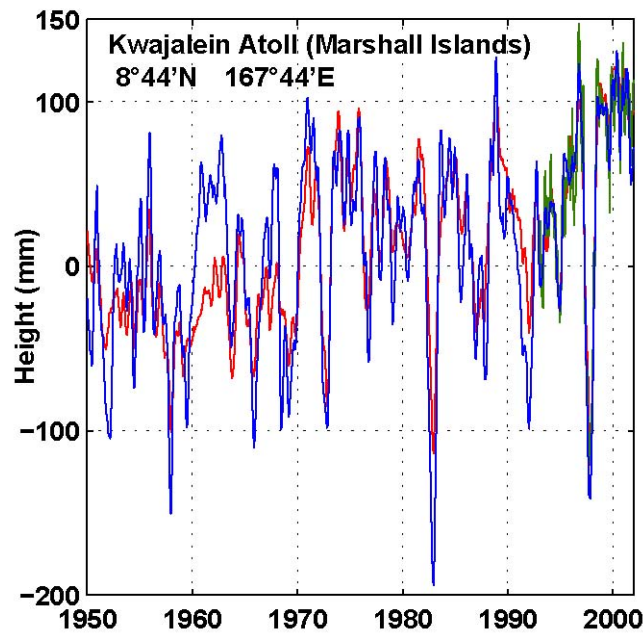10 Colors in the upper figure denote 1.6 mm/yr higher values.
11

1
2

Figure 5.5.5. Monthly mean sea level curve for 1950–2000 at Kwajalein (8°44'N, 167°44'E). The observed sea level (from tide gauge measurements) is in blue, the reconstructed sea level in red, and the satellite altimetry record in green. Annual and semi-annual signals are removed to each time series and the tide gauge curve has been smoothed. The figure was drawn using techniques in Church et al. (2004) and Church and White (2006).
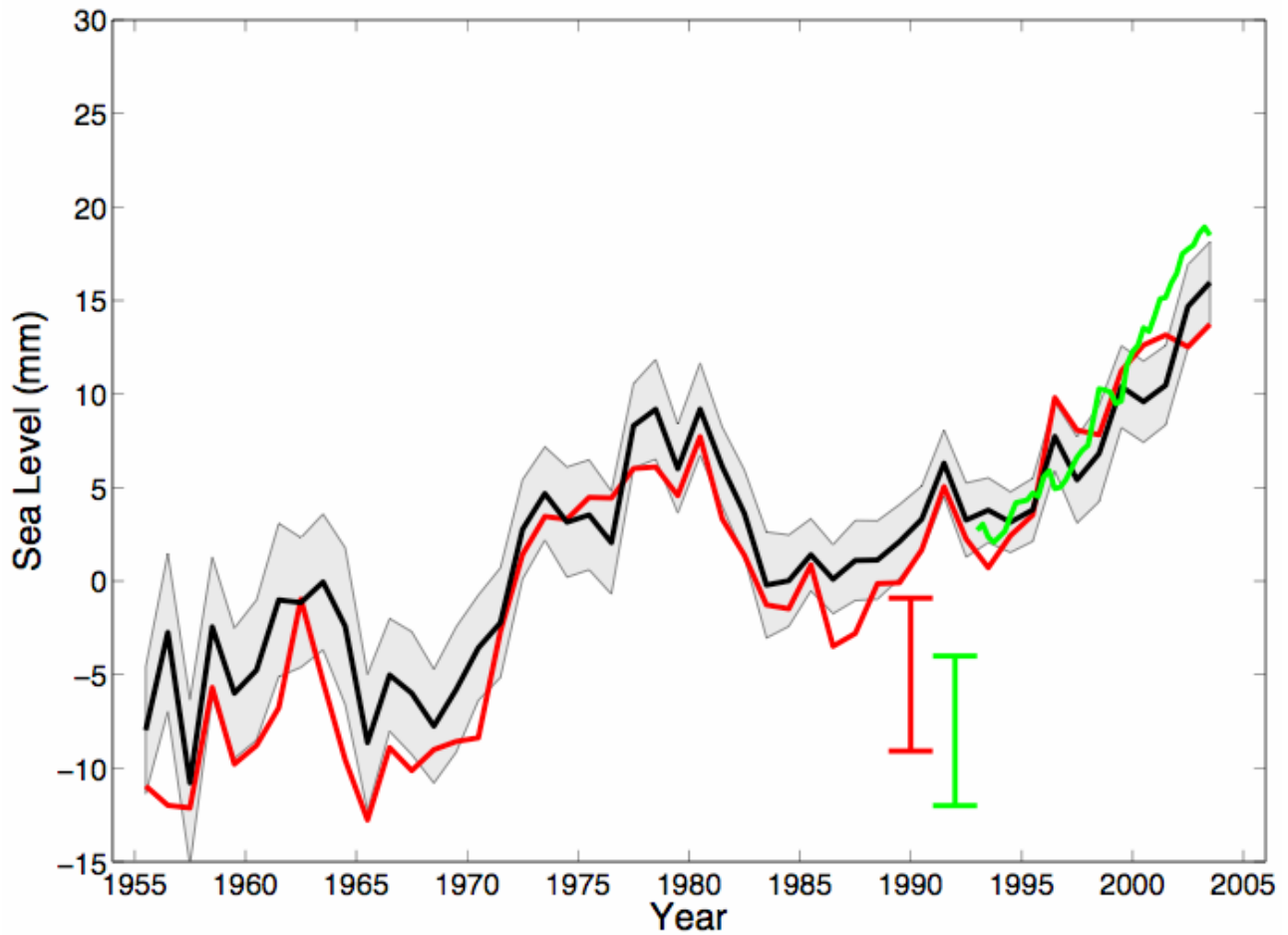
1
2

3
4
5 **Figure 5.5.6.** Thermal expansion curves based on Levitus et al. (2005a) (in black) and Ishii et al. (2006) (in
6 red), and Willlis et al. (2004) (in green) for 1955–2003, 0–700 m layer and average over 90°S–90°N. The
7 shaded area and vertical red bar represent the 95% errors of the black and red curves, respectively.
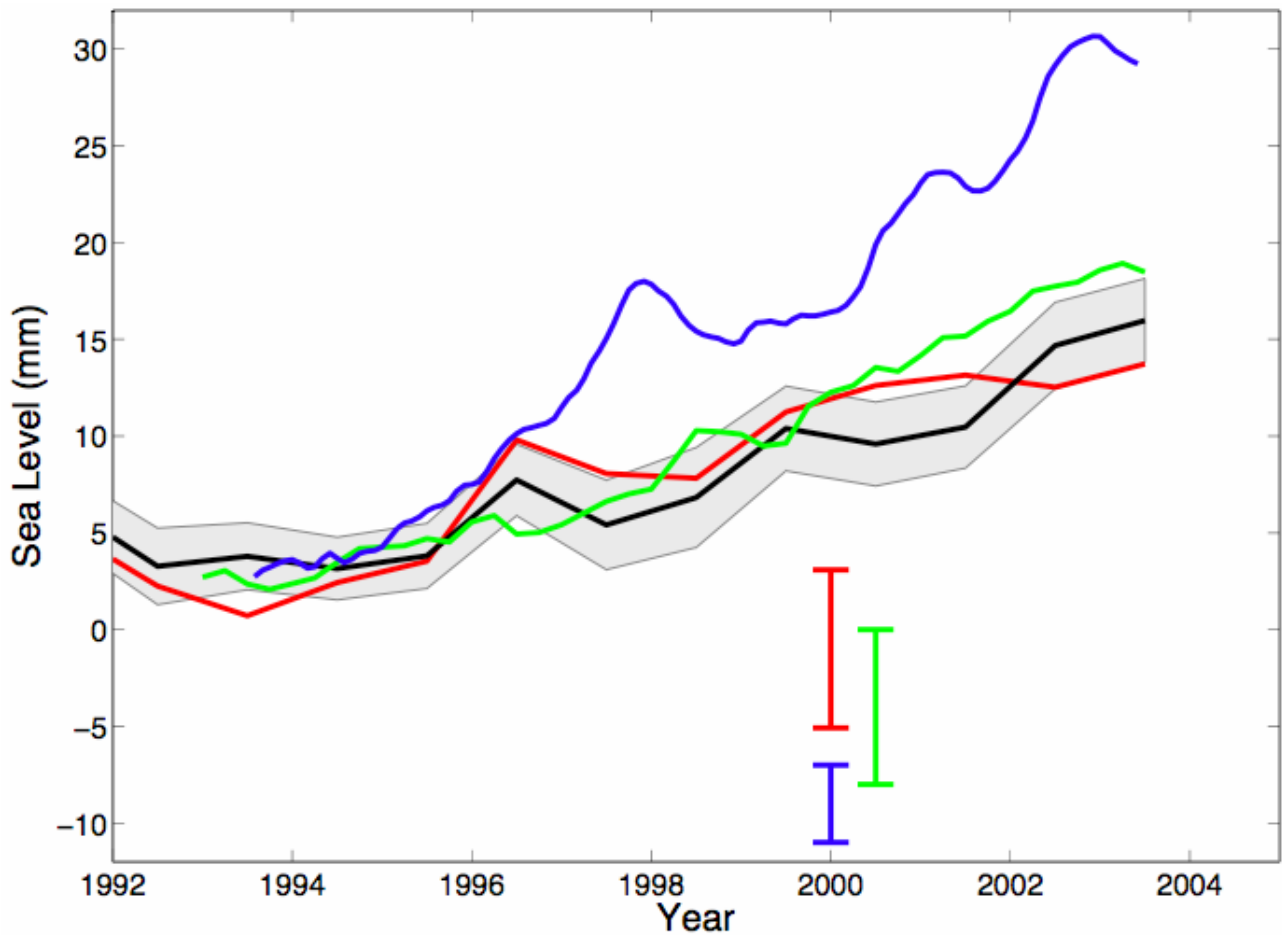8

1
2

3
4
5 **Figure 5.5.7.** Thermal expansion curves for 1993–2003, average over 60°S–60°N, based on Levitus et al.
6 (2005a) temperature data (in black; 0–700 m layer), Ishii et al. (2006) (in red; 0–700 m layer) and Willis et
7 al. (2004) (in green; 0–750 m layer). Shaded area and vertical red and green bars represent the 95% errors of
8 the black, red and green curves respectively. The blue curve is the observed global mean sea level by satellite
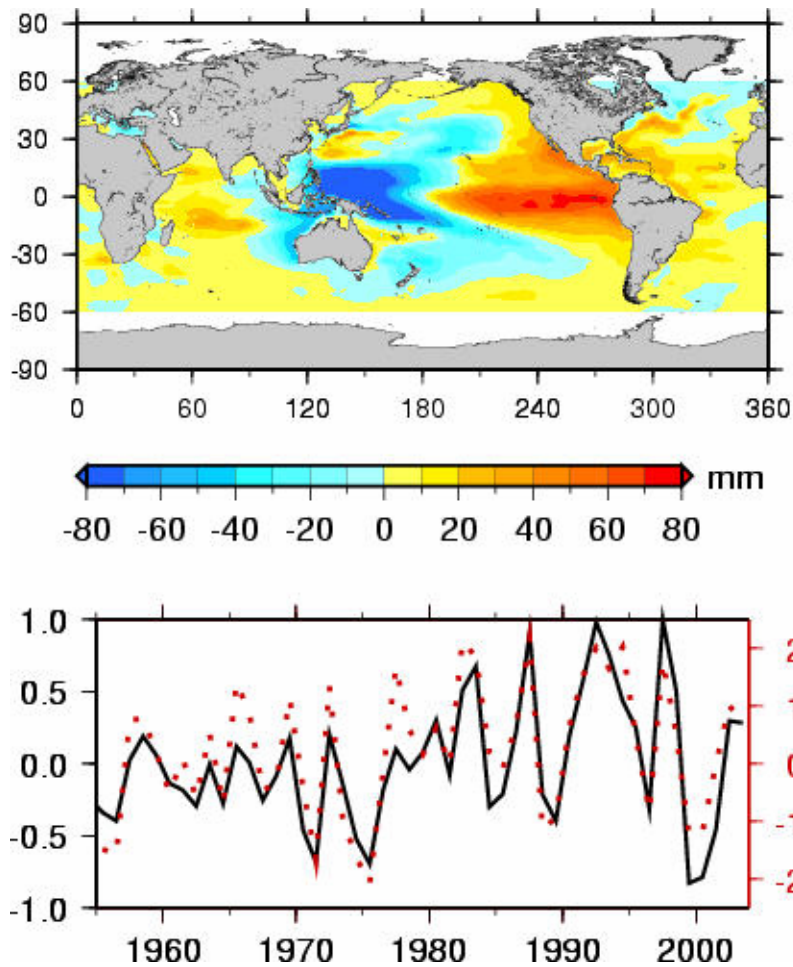9 altimetry (yearly-mean, averaged over 65°S–65°N).
10

1
2

3
4
5 **Figure 5.5.8.** First mode of the EOF decomposition of the gridded thermosteric sea level time series based
6 on Ishii et al. (2005) yearly temperature data down to 700 m. The normalized principal component (black
7 solid curve) is highly correlated with the negative southern oscillation index (dotted red curve).
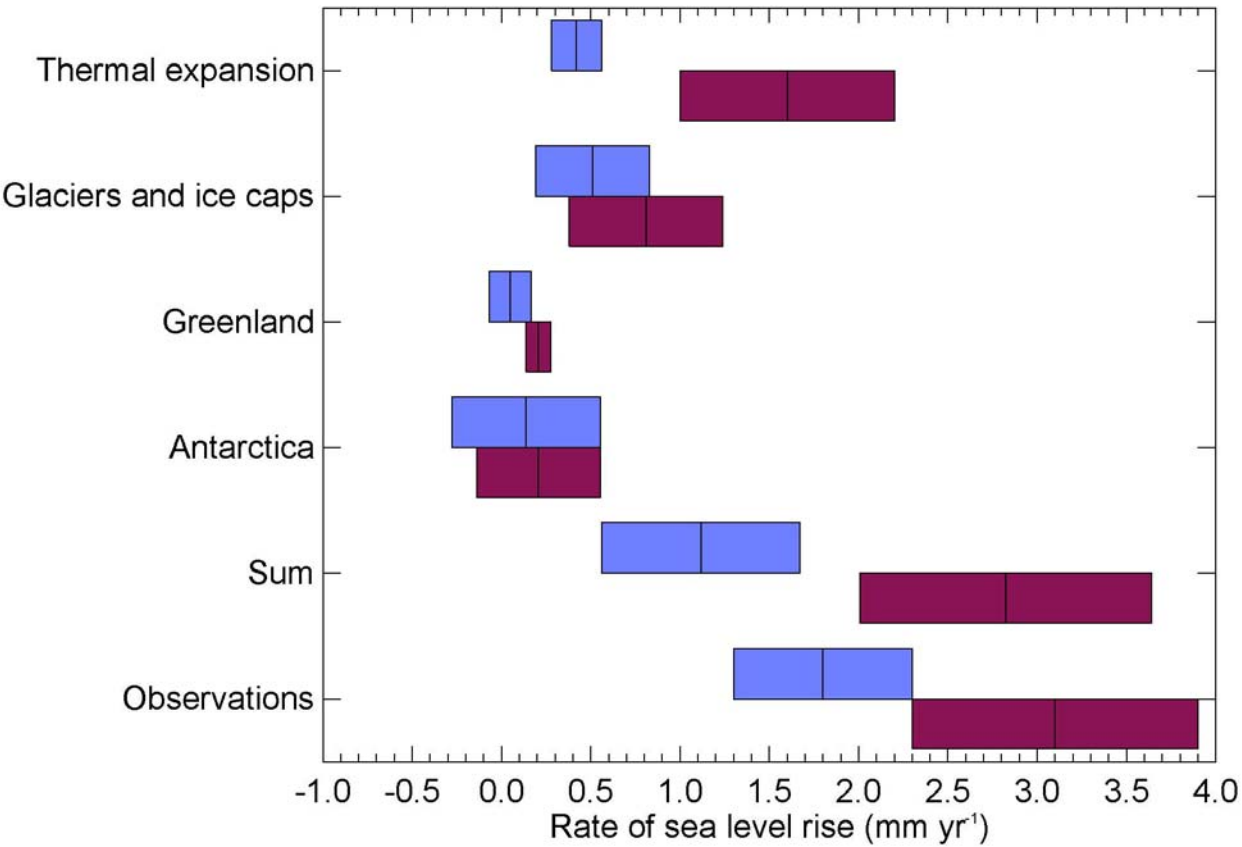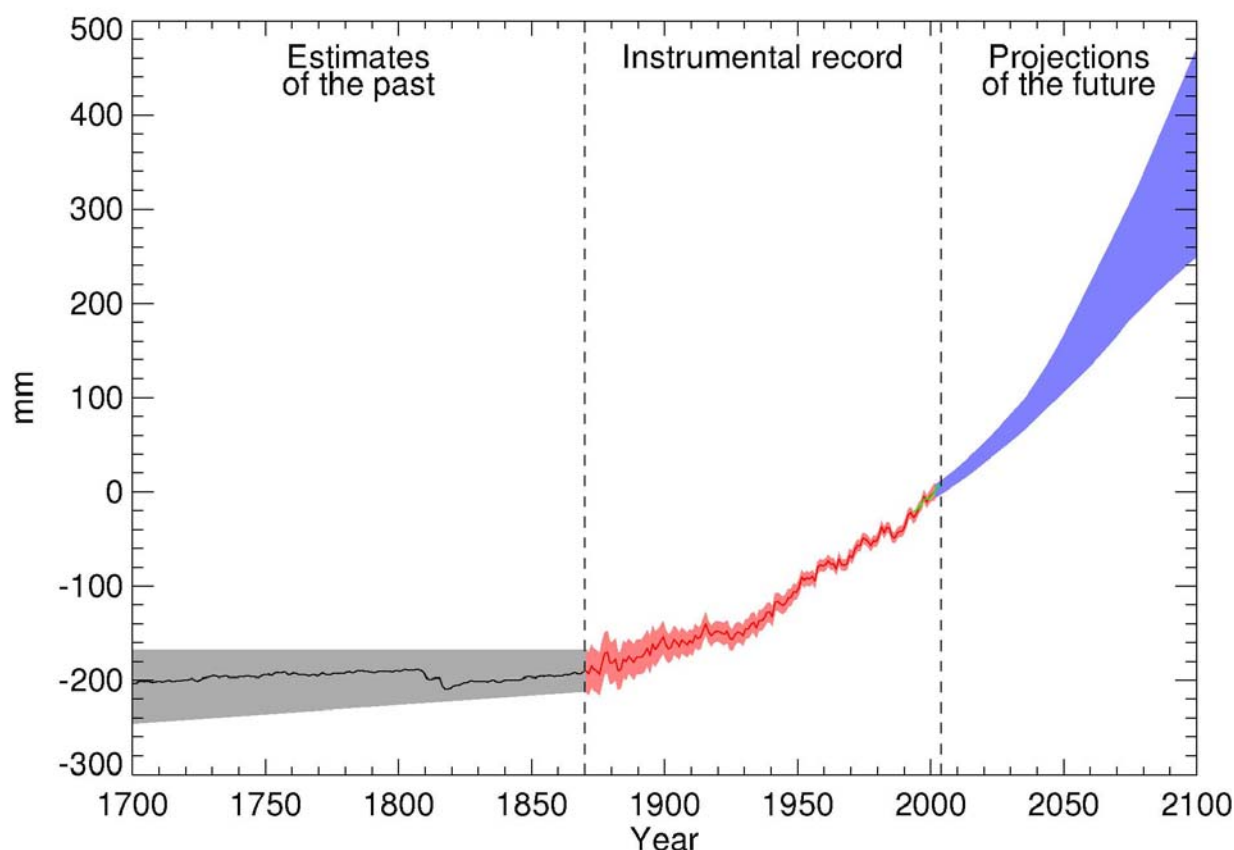8

1
2

3
4 **Figure 5.5.9.** Estimates of the various contributions to the budget of the global mean sea level change
5 compared with the observed rate of rise for 1961–2003 (blue) and 1993–2003 (red). The bars represent 95%
6 errors. The errors of the separate terms have been combined in quadrature to obtain the error on their sum.
7

1
2

3
4
5 **Question 5.1, Figure 1.** Time-series of global mean sea level in the past and future, relative to zero in 2001.
6 For the period before 1870, we do not have global measurements of sea level. The solid line here is a climate
7 model calculation (Gregory et al., 2006) of sea level change due to natural factors (volcanic and solar
8 variability) and anthropogenic factors; the rather sudden fall early in the 19th century is mainly due to the
9 eruption of Tambora in 1815. The grey shading shows the uncertainty on the estimated long-term rate of sea
10 level change (see Chapter 6, Section 6.4.3). We show a reconstruction of global mean sea-level from tide
11 gauges (Church and White, 2006, Section 5.5.2.1) for 1870-2001, with uncertainties shown by shading, and
12 from satellite altimetry (Cazenave and Nerem, 2004, Section 5.5.2.2) for 1993–2004, both as annual means.
13 For the future we indicate the range of uncertainty due to different choices of emission scenario (see Chapter
14 10, Section 10.6.5). Beyond 2100 the projections are increasingly dependent on the scenario. Over many
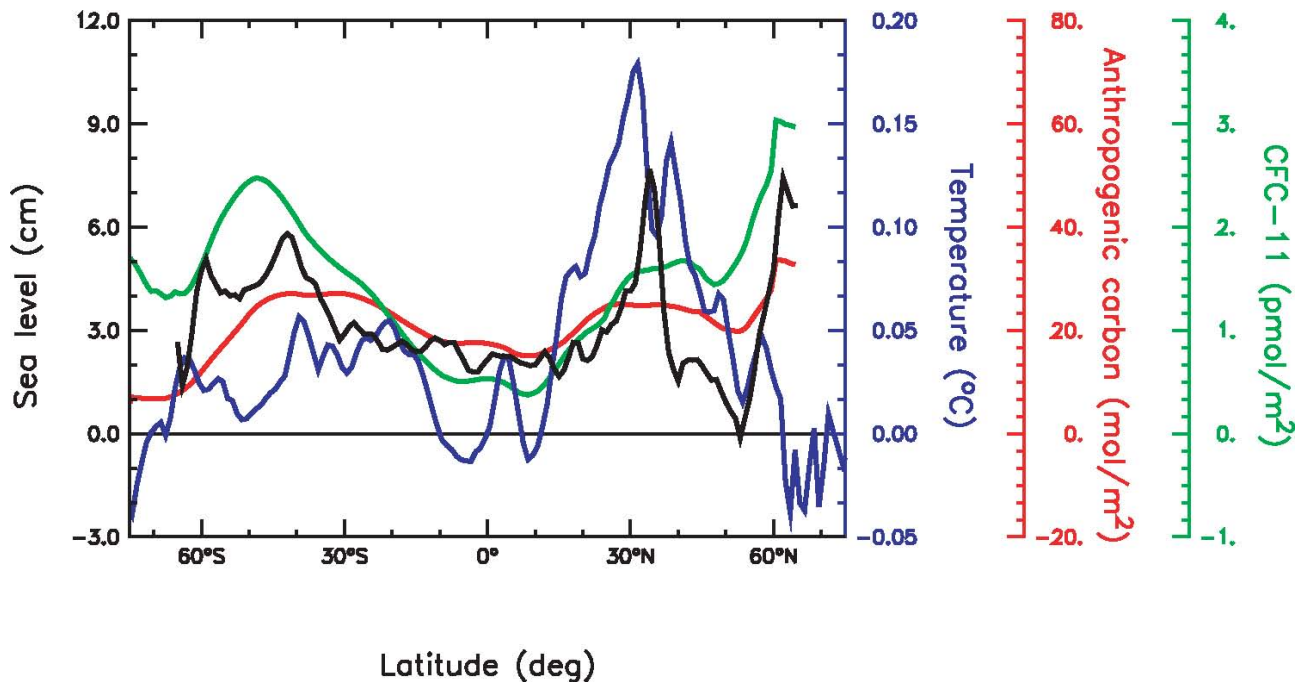15 centuries or millennia, sea level could rise by several metres (see Chapter 10, Section 10.7.3).
16

1
2

Figure 5.6.1. Averages of temperature change (blue, from Levitus et al., 2005a), Anthropogrenic CO_2 (red, from Sabine et al., 2004) and CFC-11 (green, from Willey et al., 2004) along lines of constant latitude over the top 700 m thick layer of the upper ocean. Also shown is sea-level change averaged along lines of constant latitude (black, from Cazenave and Nerem, 2004). The temperature changes are for the 1955–2003 period, the Anthropogenic CO2 is since pre-industrial times (i.e., 1750), CFC-11 concentrations are for the period 1930 to 1994, and sea-level for the period 1993 to 2003.
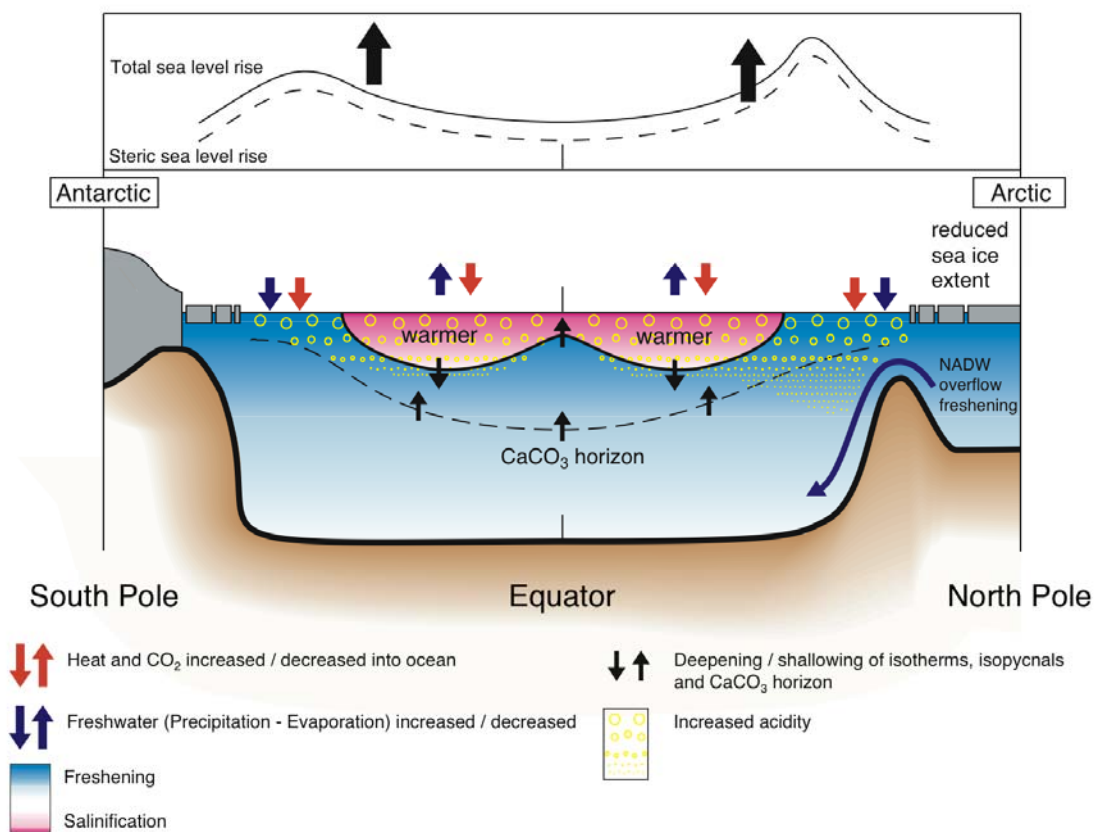
1
2

3
4
5 **Figure 5.6.2.** Schematic of the observed changes in the ocean state, including ocean temperature, ocean
6 salinity, sea-level, sea-ice and bio-geochemical cycles during the last 4-5 decades.

1
2

Number of observations= 64963

3
4

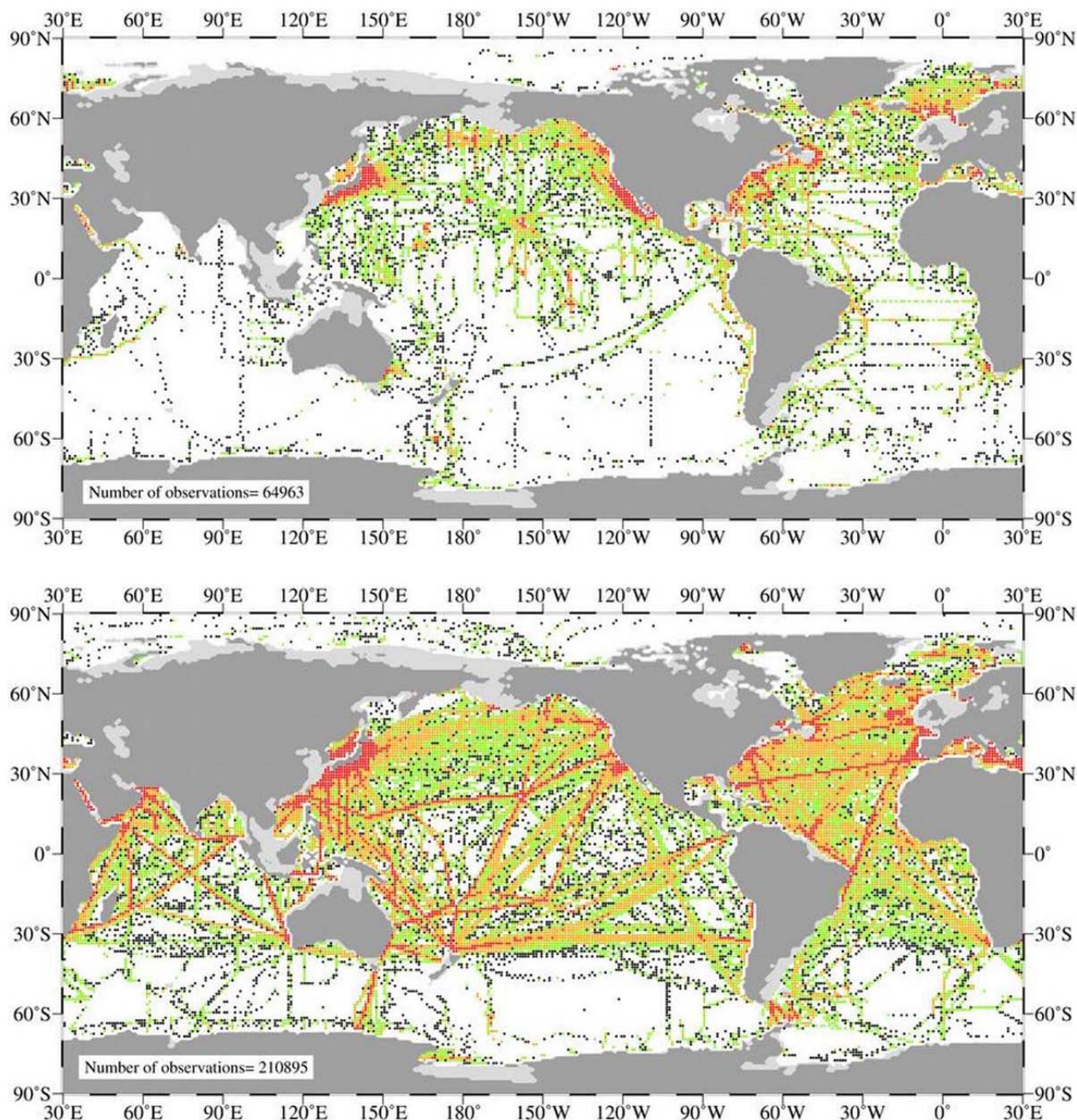Number of observations= 210895

5
6
Figure 5.A.1. Number of ocean temperature observations in each 1-degree grid box at 250 m depth for two periods, one with low and one with high density of observations. Upper figure: years 1955–1959, lower figure: years 1994–1998. A black dot indicates a 1-degree grid box containing 1 observation, green dot 2–5 observations, orange dot 6–20 observations, and a red dot greater than 20 observations.
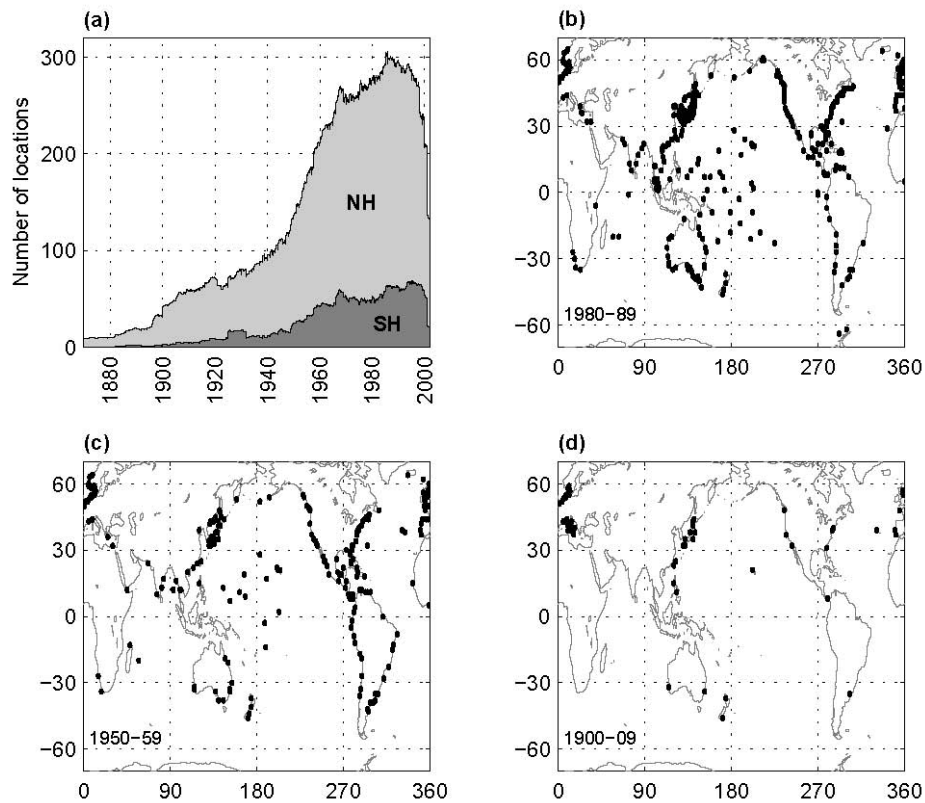
1
2

3
4
5 **Figure 5.A.2.** (a) Number of tide gauge stations in Northern Hemisphere and Southern Hemisphere used to
6 derive the global sea level curve (red curve in Figure 5.5.1), as a function of time. (b) – (d): Spatial
7 distribution of tide gauge stations for the periods 1980–1998 (b), 1950–1959 (c) and 1900–1909 (d).
8